ACS Chemical Neuroscience

Article

Radiosynthesis, Ex Vivo Biodistribution, and In Vivo Positron Emission Tomography (PET) Imaging Evaluations of [11C]2-Pyridinealdoxime Methiodide ([11C]2-PAM): A First-In-Class Antidote Tracer for Organophosphate Intoxication

Keil D. Neumann, Joseph E Blecha, Thomas R Hayes, Tony Huynh, Chih-Kai Chao, Nicolas Guilloteau, Kurt R Zinn, Henry F. VanBrocklin, Charles Mark Thompson, and John M. Gerdes

ACS Chem. Neurosci., **Just Accepted Manuscript** • DOI: 10.1021/acschemneuro.8b00212 • Publication Date (Web): 02 Aug 2018

ACS Publications

is published by the American Chemical Society. 1155 Sixteenth Street N.W., Washington, DC 20036

Revision

Radiosynthesis, *Ex Vivo* Biodistribution, and *In Vivo* Positron Emission Tomography (PET) Imaging Evaluations of [^{11}C]2-Pyridinealdoxime Methiodide ([^{11}C]2-PAM): A First-In-Class Antidote Tracer for Organophosphate Intoxication.

Kiel D. Neumann,[†] Joseph E. Blecha,[†] Thomas R. Hayes,[†] Tony Huynh,[†] Chih-Kai Chao,[‡] Nicolas Guilloteau,[‡] Kurt R. Zinn,[§] Henry F. VanBrocklin,[†] Charles M. Thompson,[‡] and John M. Gerdes*[‡]

[†]Department of Radiology and Biomedical Imaging; University of California, San Francisco; San Francisco, California, 94143, United States

[‡]Department of Biomedical and Pharmaceutical Sciences, University of Montana, Missoula, Montana, 59812, United States

[§] Departments of Radiology and Biomedical Engineering, Michigan State University, East Lansing, Michigan, 48824, United States

Revision

ABSTRACT

2-Pyridinealdoxime methiodide (2-PAM) is a widely used antidote for the treatment of organophosphorus (OP) exposure that reactivates the target protein acetylcholinesterase. Carbon-11 2-PAM was prepared to more fully understand the *in vivo* mode of action, distribution and dynamic qualities of this important countermeasure. Alkylation of 2-pyridinealdoxime with [^{11}C]CH_3I provided the first-in-class [^{11}C]2-PAM tracer in 3.5 % decay corrected radiochemical yield from [^{11}C]CH_3I , >99% radiochemical purity and 4,831 Ci/mmol molar activity. [^{11}C]2-PAM tracer distribution was evaluated by *ex vivo* biodistribution and *in vivo* dynamic positron emission tomography (PET) imaging in naïve (OP exposure deficient) rats. Tracer alone and tracer co-injected with a body mass-scaled human therapeutic dose of 30 mg/kg non-radioactive 2-PAM, demonstrated statistically similar tissue and blood distribution profiles with the greatest uptake in kidney with significantly lower levels in liver, heart and lung with lesser amounts in blood and brain. The imaging and biodistribution data show that radioactivity uptake in brain and peripheral organs is rapid and characterized by differential tissue radioactivity washout profiles. Analysis of arterial blood samples taken 5 min after injection showed ~82% parent [^{11}C]2-PAM tracer. The imaging and biodistribution data are now established enabling future comparisons to outcomes acquired in OP intoxicated rodent models.

Revision

KEYWORDS

2-pyridinealdoxime methiodide (2-PAM)

antidote

biodistribution

carbon-11

organophosphate

PET imaging

INTRODUCTION

The therapeutic agent 2-pyridinealdoxime methiodide (2-PAM, pralidoxime; Figure 1) is widely accepted as an antidote therapy in the US for the reactivation of acetylcholinesterase (AChE) that has been inhibited by organophosphorus compounds such as chemical warfare agents and certain insecticide oxons (Scheme 1).[1-3] The combination of 2-PAM with other centrally-acting drugs such as a muscarinic blocker (e.g., atropine[4]) and anti-seizure medication (midazolam[5, 6]) along with other supportive regimens define the standard of care for OP exposures, including self-poisoning.[7]

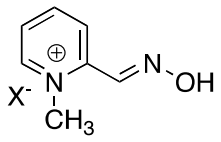

X = I; 2-PAM
X = OMs; P2S

Figure 1. Chemical structures of the pyridine aldoximes.

Revision

Scheme 1. Inhibition of acetylcholinesterase by organophosphorus compounds and reactivation of the OP-AChE adduct by 2-PAM.

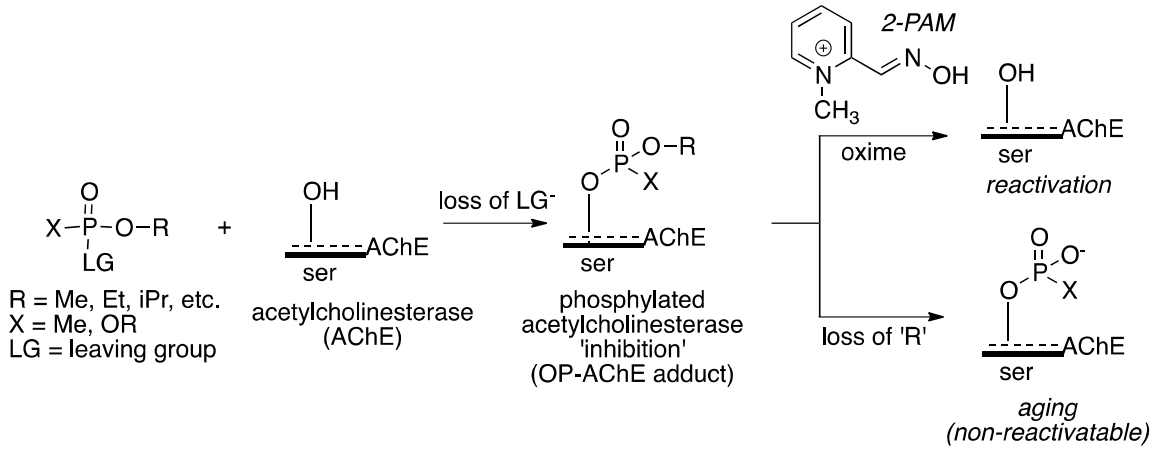

The mechanism by which 2-PAM or P2S (the analogous methanesulfonate salt), in addition to other select oximes, regenerates acetylcholinesterase enzymatic activity occurs via nucleophilic displacement at the phosphorus atom of the serine-O-phosphoryl linkage (Scheme 1) by the oxime C=N-OH moiety. The charged pyridinium ring of 2-PAM plays a supportive role in this mechanism as it is believed to initially guide the antidote to the cation-attracting, peripheral binding domain of AChE and aids docking in the active site similar to that achieved by the natural substrate acetylcholine that also bears a quaternary amine. As an antidote therapeutic to OP intoxication, 2-PAM reacts selectively with OP-modified AChE and other OP-adducted esterases. In the absence of OP-AChE and esterase modifications, 2-PAM is without a specific high affinity *in vivo* target.

Despite the favorable role of the cation moiety in the enzyme activity restoration mechanism, it is believed that cationic 2-PAM is primarily distributed to peripheral tissues because the blood–brain barrier (BBB) impedes facile diffusion

Revision

of the cationic antidote into the central nervous system (CNS).[8, 9] Diminished CNS access by charged therapeutic agents such as 2-PAM limits their usefulness. However, select studies reported that 2-PAM does reactivate OP-modified AChE in rat brain.[10] In support of that work, Sakurada and colleagues reported that 2-PAM enters rat brain in a dose-dependent manner in the absence of OP treatment using microdialysis measures.[11] Additionally, it has been shown that [^{14}C]2-PAM enters brain more readily following exposure to the OP trichlofon (Dipterex; O,O-dimethyl, 2,2,2-trichloro-1-hydroxyethyl phosphonate).[10, 12] Although low concentrations of 2-PAM can enter brain, it remains less clear how brain levels might vary over time within the first hour of 2-PAM administration, as a function of the absence or presence of OP exposure. In an effort to further interrogate 2-PAM brain penetration under these and related conditions, we sought to generate and initially evaluate carbon-11 ($t_{1/2}$ = 20.4 min) radiolabeled 2-PAM ([^{11}C]2-PAM) tracer that would enable facile *ex vivo* and *in vivo* CNS and peripheral tissue determinations.

The [^{11}C]2-PAM tracer was considered ideal for preliminary assessments of pharmacokinetic (PK) properties in rat CNS and peripheral tissues by *ex vivo* biodistribution (bio-d) and *in vivo* positron emission tomography (PET) imaging evaluations. The acquired tracer data would ultimately enable correlation to previously established 2-PAM biochemical and toxicological study outcomes.[1-3, 7, 11-14] In this study, we report the radiosynthesis of a first-in-class [^{11}C]2-PAM tracer and initial evaluations of the tracer using naïve rats that have not undergone OP exposure. The assessments include *ex vivo* bio-d measures,

Revision

blood metabolite assessment and *in vivo* PET imaging determinations after administration of tracer alone (baseline profiles). Additionally, we describe select experiments, in which a therapeutic dose level of non-radioactive (cold) 2-PAM was co-administered with the tracer. Together, the naïve rat [^{11}C]2-PAM tracer profiles serve as fundamental data for comparisons to related future tracer measures in OP intoxicated rats.

RESULTS AND DISCUSSION

The high molar activity radiosynthesis of [^{11}C]2-PAM was developed based on literature precedent[15] from the readily accessible radiolabelling synthon [^{11}C]methyl iodide ([^{11}C]CH_3I)[16] and 2-pyridinealdoxime, such that the tracer could be generated by a one-step alkylation procedure (Scheme 2). Special considerations were taken using the [^{11}C]CH_3I approach since most cold preparations of N-methyl pyridinium ions use a large surplus of the alkyl iodide and long reaction times relying on precipitation of the salt for isolation. Preliminary cold chemistry studies using a large inverse ratio of 10- to 50-fold 2-pyridinealdoxime relative to methyl iodide revealed that a high conversion (> 80% based on methyl iodide as the limiting reagent) to 2-PAM could be accomplished in less than 5 min at 120 ˚C in dimethylformamide (DMF). Acetonitrile (CH_3CN) was also found as a suitable solvent and led to ~ 40% conversion to cold product under similar conditions. Methylation in other solvents such as DMSO, N-methylpyrrolidine, and dimethoxyethane (DME) were found to be less effective than DMF or CH_3CN when a surplus of 2-pyridinealdoxime was used. The non-

Revision

radioactive reaction yield in either DMSO or CH_3CN was not improved at temperatures below 90 ˚C nor above 120 ˚C (sealed tube conditions).

Scheme 2. Radiosynthesis of tracer [^{11}C]2-PAM.

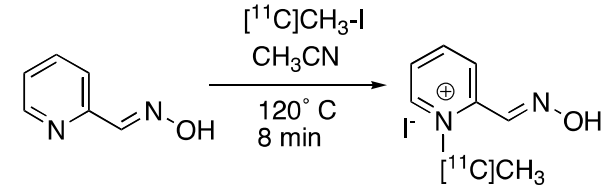

Pyridine-2-aldoxime ***[^{11}C]2-PAM***

Adaptation of the modified cold synthetic route to the corresponding radiosynthesis required [^{11}C]CH_3I, which was prepared by an established gas-phase automated method.[16] In this approach, [^{11}C]CH_3I was bubbled into a solution of 2-pyridinealdoxime (1 mg) in CH_3CN, the reaction vessel was sealed and heated at 120 ˚C for 8 min, then cooled briefly, diluted with saline and the tracer was purified by reversed-phase high performance liquid chromatography (HPLC). The rapid formation of [^{11}C]2-PAM occurred in a decay-corrected radiochemical yield of 3.5 ± 0.9 % (n = 8), relative to [^{11}C]CH_3I with a measured molar activity of 4,831 ± 911 Ci/mmol (n = 8), >99% radiochemical purity, and in a total synthesis time of 40 min from delivery of [^{11}C]CH_3I. A similar protocol using DMF as the reaction solvent at 140 ˚C afforded a higher decay-corrected tracer yield (16.5 ± 6.5%, n = 3) relative to [^{11}C]CH_3I; yet, purification by HPLC was difficult when DMF was used as reaction solvent, resulting in a lower tracer radiochemical purity (85-90%, see: Supporting Information). A limited series of reactions was conducted in an attempt to increase the yield of [^{11}C]2-PAM using

Revision

CH_3CN as the reaction solvent. Adjusting temperature (80-120˚C) and mass of precursor (5-10 mg) did not afford an improved yield of [^{11}C]2-PAM (per Supporting Information, Additional Labeling Studies for [^{11}C]2-PAM Preparation, Table S1). Since the use of CH_3CN solvent was superior for gaining higher final tracer purity, albeit affording tracer in lower radiochemical yield, the CH_3CN protocol was used for the reported preclinical studies. Tracer doses, formulated in ~ 1 mL sterile isotonic saline, were found to be stable for > 2 h at room temperature by HPLC analysis and up to 10 mCi (non-decay corrected) of final formulated [^{11}C]2-PAM tracer was typically achieved.

To initially appraise CNS and peripheral tissue tracer uptake profiles, bio-d determinations and PET imaging studies were performed using 250-400 g (mean body weight 305 g) male Sprague-Dawley rats (n = 3 per group) that were administered [^{11}C]2-PAM by tail vein intravenous (i.v.) injection under light isoflurane (1-2%) anesthesia. Biodistribution experiments used 100-200 μCi tracer doses (1.0-1.5 mL) where the initial studies were carried out with tracer alone (baseline conditions). Baseline *ex vivo* biodistribution radioactivity profiles (blood and tissues) were sampled at select 2-60 min time points after tracer injection (Figure 2), for blood, brain, liver, heart, kidney and bone (femur). The samples were counted affording data as decay-corrected percent injected dose radioactivity per gram tissue values (% ID/g) ± standard error measures (SEM). The bio-d radioactivity profiles reveal highest uptake in kidney with significantly diminished amounts in liver, lower uptake in lung and heart, and the lowest radioactivity in blood, brain and bone. For all samples, time-dependent

Revision

radioactivity uptake and washout profiles were observed for the tissues and blood over 60 min. The rapid radioactivity uptake and washout seen within naïve rat tissues (i.e., lack of an OP-AChE modification) are consistent with the absence of a high affinity 2-PAM target within the tissues and blood.

The elevated radioactivity in kidney at 2 and 5 minutes was anticipated for a cationic, highly water soluble compound and thought to be associated with clearance.[17, 18] Limited brain radioactivity uptake observed at all times is considered to be a function of the diminished ability of cationic [^{11}C]2-PAM (and/or related species) to diffuse across the BBB.[11, 12] Applying the average-sized rat brain blood volume of ~ 30-35 μL/g of tissue[19] for the blood and brain % injected dose (ID) per gram profiles over time (Figure 2), indicates that ~ 8-15 % of the brain radioactivity detected over the 2-60 minutes is contributed from the cerebral blood pool radioactivity within brain tissue. Thus, the majority of the brain radioactivity (Figure 2) is associated with tissue (see Methods section and Supporting Information).

Revision

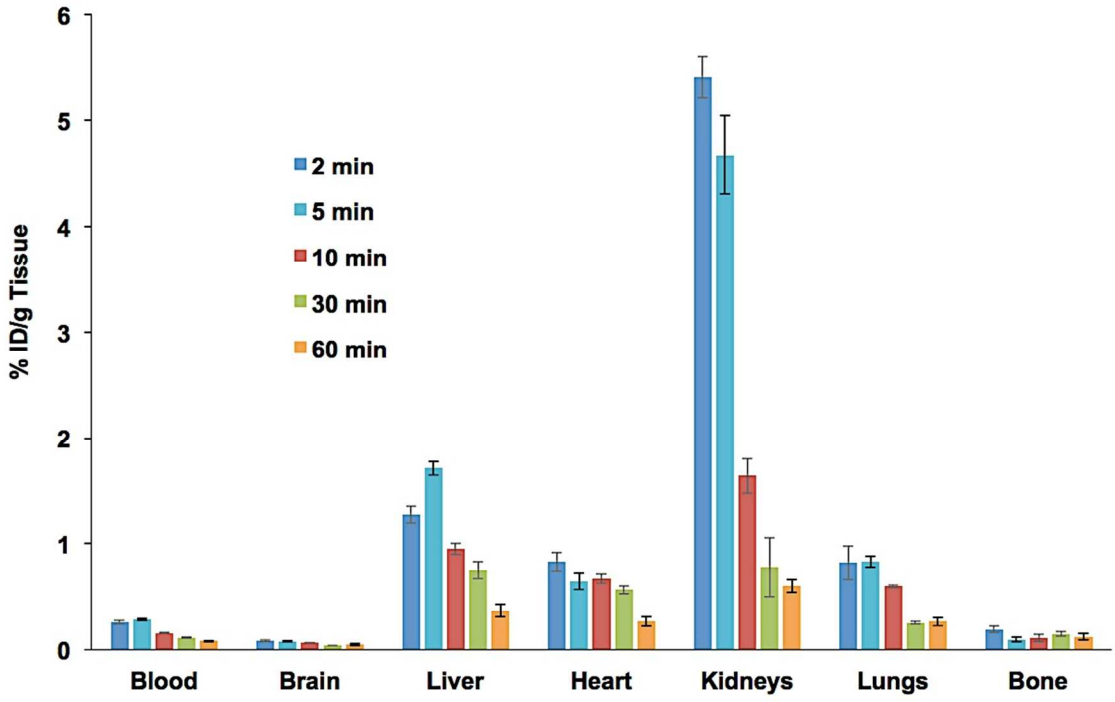

Figure 2. Mean baseline (tracer alone, n = 3, ± SEM) biodistribution (2-60 min) of decay-corrected radioactivity after [^{11}C]2-PAM tracer i.v. injection in naïve rats.

Tracer metabolism events are thought to contribute to the liver radioactivity levels (Figure 2).[12, 20] Since the highest liver radioactivity was observed at 5 min, evaluation of blood non-protein-bound fraction components was conducted to assess the amount of parent tracer activity relative to metabolites. Tail artery blood sampling at 5 minutes, blood sample processing and chromatographic profiling against non-radioactive (cold) chemical metabolite standards afforded a distribution of radioactivity components (Figure 3). At 5 minutes after tracer injection, the non-protein-bound fraction showed 82.3% parent [^{11}C]2-PAM tracer and a mixture of metabolites including 4.4% N-methyl-2- pyridinecarboxaldehyde,

Revision

4.7% of a mixture of N-methyl-2- pyridinecarboxamide, N-methyl-2-pyridinecarboxylic acid, N-methyl-2-pyridinecarbonitrile, and 8.6% N-methyl-2-pyridone (Figure 3). The metabolite structures and relative distribution are consistent with 2-PAM metabolites reported previously,[12, 15, 20] albeit with some minor differences that could result from dose sizes and rat strains. The Figure 3 metabolism results provide insight into the maximal 5 min liver bio-d profile. At present it remains unclear whether uptake of the metabolites into brain occurs, are produced in brain, or both.

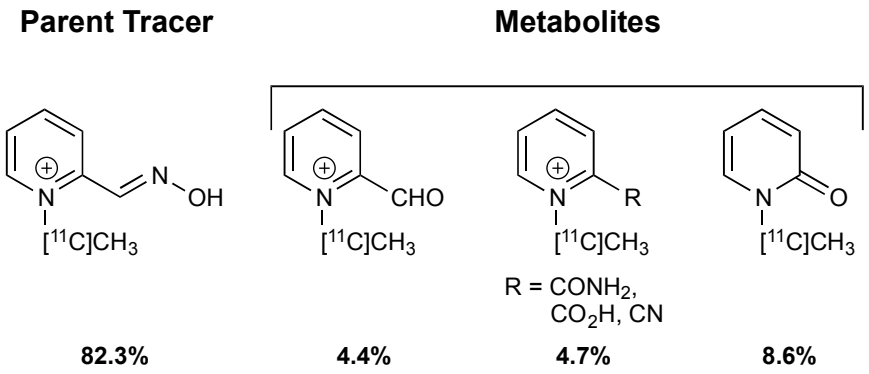

Figure 3. Plasma free-fraction relative radioactive components determined by chromatographic separation and counting at 5 min after tracer injection.

We sought to further interrogate the 5 min bio-d time point since previous studies with 2-PAM have shown a dose-dependent increase in brain penentration.[11] Our initial appraisal used tracer that was co-injected with a 30 mg/kg of cold 2-PAM dose that is akin to a human 30 mg/kg therapeutic 2-PAM dose,[1, 3, 11] where the total mass of cold 2-PAM injected was not allometrically scaled. The experiment was designed to compare the presence vs. absence of

Revision

cold 2-PAM in relation to activity uptake and washout profiles in naïve rats in the absence of an OP-AChE modification. Further, differential tracer tissue interactions associated with metabolism, clearance or other processes might also be detected in the presence of cold therapeutic agent. The results are shown in Figure 4 with baseline (tracer alone) versus 30 mg/kg cold 2-PAM dose co-injected with tracer. One-way ANOVA analyses show no significant differences between the two tracer dose regimens, [^{11}C]2-PAM only (baseline) versus tracer in the presence of 30 mg/kg cold 2-PAM, in most of tissue activity distributions at 5 min except the liver ($P = 0.0085$). The significant elevated liver activity in the presence of cold 2-PAM is thought to be a result of altered tracer metabolic processes. No significant difference in 2-PAM brain radioactivity uptake between tracer alone and tracer plus therapeutic cold 2-PAM dose experiments were found, suggesting that the uptake was not effected by mass dose level. With the exception of liver and in the absence of OP-AChE modification, the naïve rat activity biodistribution PK profiles resulting from [^{11}C]2-PAM tracer low mass doses (Figure 4) are thought to be similar to those of higher mass doses of non-radioactive 2-PAM.[17, 18]

Revision

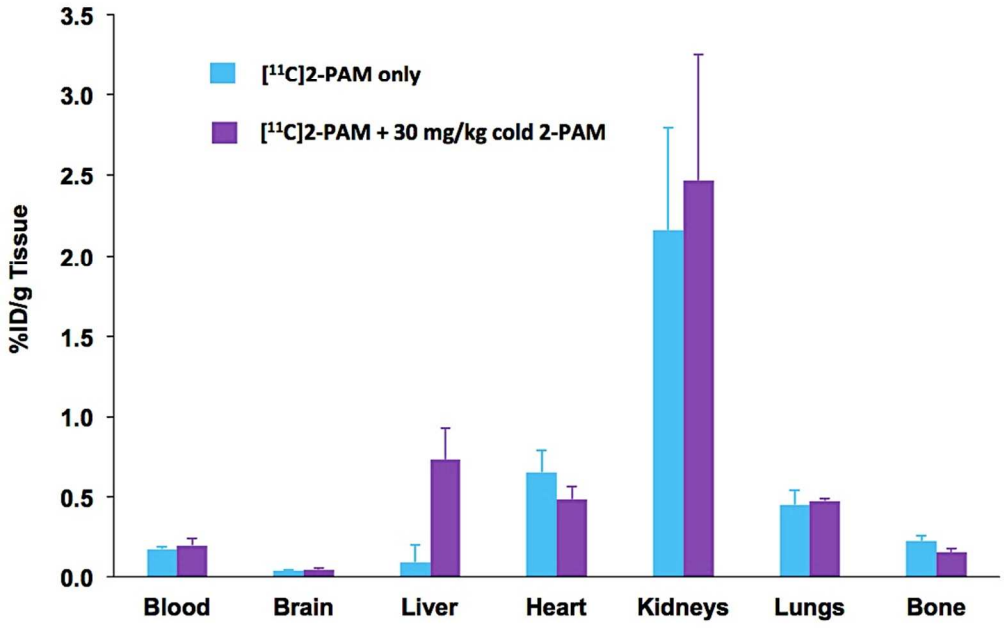

Figure 4. Comparison of the mean (n = 3, ± SEM) radioactivity (decay- corrected) biodistributions of baseline [^{11}C]2-PAM (tracer alone, aqua) and [^{11}C]2-PAM co-injected with 30 mg/kg cold 2-PAM (purple) at 5 min after respective tracer i.v. injections in naïve rats.

To distinguish the *in vivo* radioactivity tissue distributions in naïve rats, 30 min dynamic *in vivo* PET scanning (5 min frames) was employed that used 0.5-1.0 mCi tracer i.v. doses. The 30 min scan time was based on the rapid activity uptake and washout defined by the bio-d profiles (Figure 2). The PET scans were carried out to afford *in vivo* data for comparison to the *ex vivo* biodistribution profiles. The PET imaging was carried out in parallel with micro-computed axial tomography (CT) and magnetic resonance (MR) scanning for the sake of anatomical tissue information and data co-registration allowing for conservatively defined volumetric three-dimensional regions of interest (ROIs) relative to

Revision

established rat brain and peripheral tissue atlas designations.[21-23] Regional radioactivity signals were determined as standardized uptake values (SUV, per Methods section)[24] that permitted imaging evaluations across rats for determinations of the mean (n = 3) SUV values ± SD per ROI vs. time (min). The resultant tracer baseline and tracer in the presence of cold 2-PAM time-activity curves (Figure 5) and expanded the brain TAC data (Figure 6) were obtained. A typical sagittal PET view of summed radioactivity co-registered with CT data, after baseline [^{11}C]2-PAM tracer injection is depicted in Figure 7.

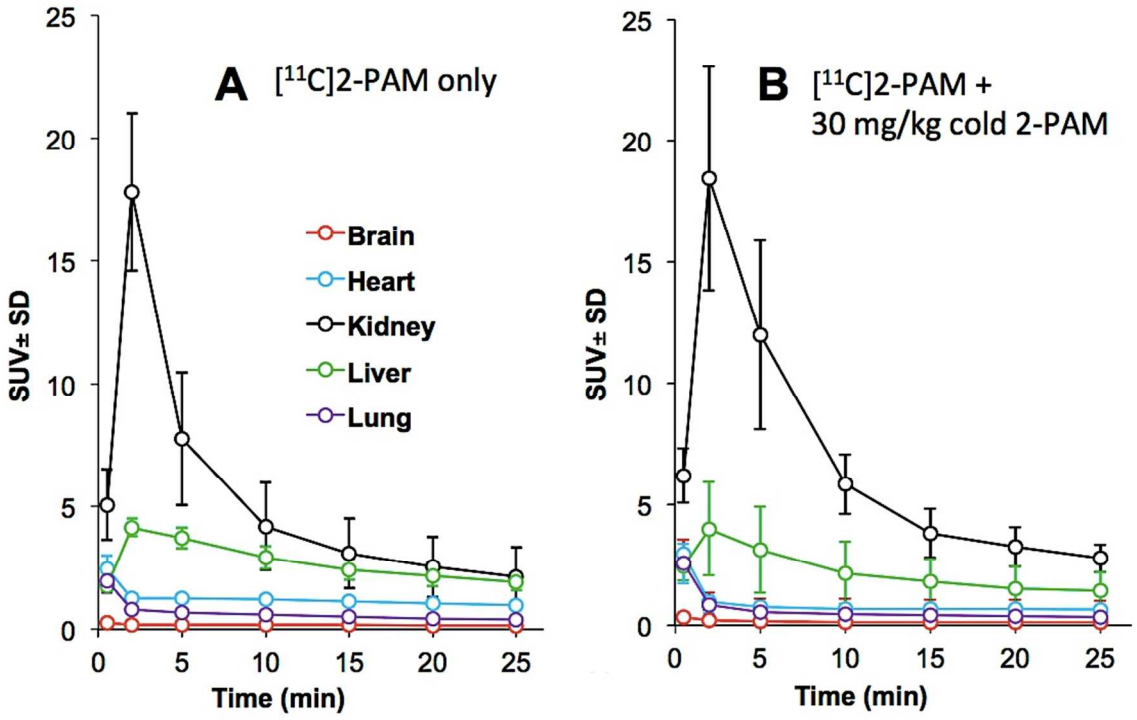

Figure 5. The mean values (n = 3, ± SD) PET imaging detected radioactivity (decay corrected and subject normalized as SUV) vs. time (min) curves in naïve rats after [^{11}C]2-PAM tracer: Panel A, tracer alone (baseline) and Panel B, tracer

co-injected with 30 mg/kg cold 2-PAM (see Supporting Information for expanded plots of these curves).

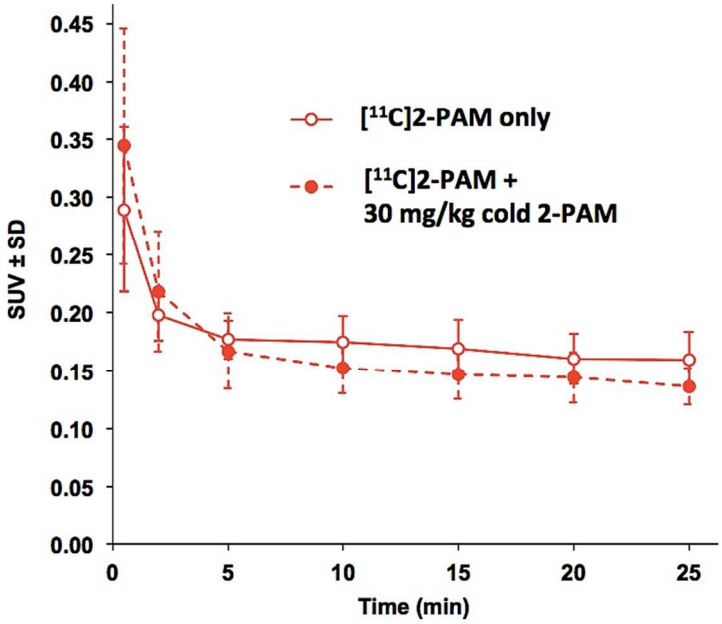

Figure 6. Expanded view PET imaging brain time-activity curves of mean SUV (n = 3, ± SD) vs. time (min) for [^{11}C]2-PAM tracer alone (baseline; open circles and solid line) and tracer co-injected with 30 mg/kg cold 2-PAM (solid points and dashed line).

Revision

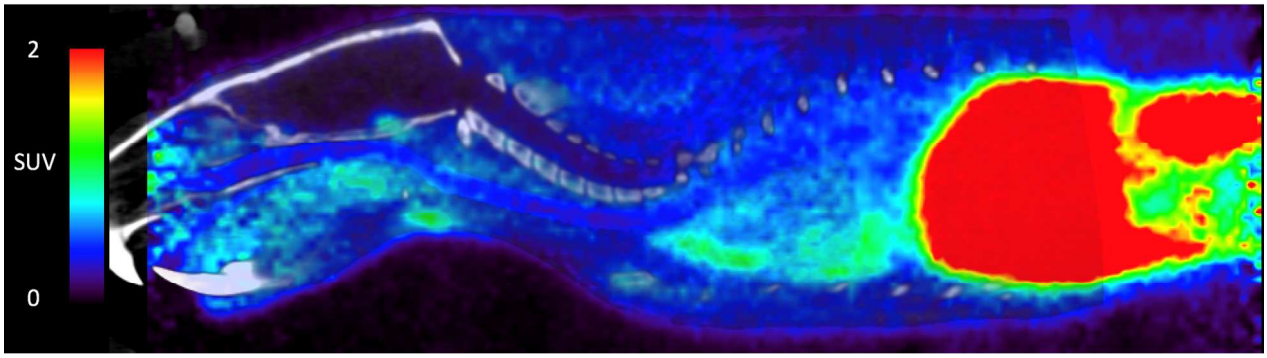

Figure 7. A PET-CT sagittal (cranial, rostral left; caudal right) view near mid-line (MR data omitted for clarity) of 30 min summed activity (SUV color bar) after injection of 0.95 mCi of [^{11}C]2-PAM tracer alone (baseline) in a male 330 g rat.

Baseline PET imaging TAC plots (Figure 5, Panel A) show high radioactivity in kidney, less in liver, low levels in heart and lung and lower level activity in whole brain. These relative *in vivo* SUV profiles are similar to the *ex vivo* biodistribution radioactivity determinations (Figure 2). An analogous assessment was made when [^{11}C]2-PAM was co-injected with 30 mg/kg of cold 2-PAM (Figure 5, Panel B) showing the similarity (Panel A vs. Panel B) and significant amounts of radioactivity washout by 25 min after tracer injection. The relative distributed amounts of radioactivity detected (Figure 5, Panel A and B) are found similar to the *ex vivo* bio-d profiles of Figure 2; that is, radioactivity distribution profiles as kidney >> liver > heart, lung > brain. The elevated radioactivity found in kidney and liver as compared to heart and lung (Figure 5) likely represents greater tissue reservoirs for 2-PAM (and related radiolabeled species) associated with clearance

Revision

and metabolism, respectively. The Figure 5 mean radioactivity liver values at five minutes after tracer injection do not clearly show a distinction between the Panel A (tracer alone) vs. Panel B (tracer in the presence of 30 mg/kg cold 2-PAM), whereas differences are found from the similar liver bio-d determinations as shown in Figure 4. The reasons for the differences remain unclear. The expanded naïve rat brain TAC plots (Figure 6) for baseline and the co-injection of cold 2-PAM experiments reveal that the curves are not significantly different from each other. Radioactivity enters brain rapidly, albeit at low levels, and reaches a steady concentration in brain after 5 min. Low brain radioactivity uptake was anticipated based on previous biodistribution reports using naïve rats.[11, 12]

The PET imaging results demonstrate that the use of the short carbon-11 half-life [^{11}C]2-PAM tracer within naïve rats is suitable for quantitatively detecting radioactivity PK uptake and washout changes in tissues of interest. The baseline PET data reveals radioactivity distributions that are relatively uniform relative to the *ex vivo* time-activity biodistribution determinations. Within naïve rat tissues, the PET TAC data from the co-injection of non-radioactive 2-PAM is similar to baseline profiles, which we consider consistent for the naïve rat condition that is devoid of an OP-AChE adduct (Scheme 1) thereby lacking a high affinity 2-PAM target.

CONCLUSIONS

To gain deeper insights into the pharmacokinetic properties of the therapeutic antidote 2-PAM, the first-in-class [^{11}C]2-PAM tracer was selected for study initially within naïve (OP exposure deficient) rats that lack a high affinity *in*

Revision

vivo target for the tracer. The tracer was prepared by a straightforward approach using a one-step alkylation reaction with [^{11}C]CH_3I followed by HPLC purification, providing stable (2 h) saline-formulated dose preparations that were administered intravenously. Initial uptake and washout radioactivity PK assessments within CNS and peripheral tissues, and also blood, were made by *ex vivo* biodistribution profiling over 60 min. Radioactivity distributions were realized for baseline (tracer alone) and at the selected 5 min time with tracer co-injected with cold 2-PAM (human therapeutic dose level, 30 mg/kg). A range of high to low radioactivity was found in blood and tissues; respectively, kidney >> liver > lung and heart >> blood, brain and bone. The high kidney radioactivity was anitcipated for a water soluble cationic compound, and similarly, the low brain activity was expected based on the diminished ability of cationic species to diffuse across the BBB. Realizing the liver activity maxima at 5 min could be related to previously described 2-PAM metabolic transformations, and that this activity level was affected by cold 2-PAM co-administration, arterial blood collection under baseline conditions at 5 min and subsequent processing revealed plasma free-fraction activity components as 82.3% parent [^{11}C]2-PAM tracer and just 17.7% as cognate metabolites previously described in the literature.

Dynamic *in vivo* PET imaging for 30 min using [^{11}C]2-PAM tracer under baseline condtions and also tracer co-injected with 30 mg/kg cold 2-PAM revealed CNS and peripheral tissue radioactivity distributions that were relatively similar to the time-activity profiles established by the *ex vivo* biodistribution experiments. The non-radioactive 2-PAM plus tracer conditions were found without significant

Revision

differences on brain radioactivity profiles over 30 min, which was expected for naïve rats that lack a high-affinity OP-AChE adduct target. The PET imaging confirms low radioactivity uptake into brain as previously described in the literature for non-radioactive 2-PAM. In summary, the naïve rat *ex vivo* biodistribution and *in vivo* PET imaging time-activity measures after [^{11}C]2-PAM tracer i.v. injection serve as fundamental correlated data sets. This requisite data is now poised to enable meaningful comparisons relative to tracer determinations in OP-intoxicated rats in which the detection of [^{11}C]2-PAM participation in the critical therapeutic regeneration of acetylcholinesterase activity will be probed.

METHODS

General. Reagents (e.g., 2-pyridinealdoxime, iodomethane, *et al.*), solvents such as anhydrous dimethylformamide (DMF), anhydrous acetonitrile (CH_3CN), and 2-pyridinealdoxime methiodide were reagent grade or better, used without any additional purification, and were purchased from Sigma Aldrich Chemical Company (Milwaukee, WI). USP-grade sterile isotonic saline was also purchased from Sigma-Aldrich. 2-Pyridinecarboxaldehyde, 2-pyridinecarboxamide, 2-pyridinecarboxylic acid and 2-pyridinecarbonitrile were converted into the N-methyl pyridium metabolite standards per literature methods.[25, 26] Nuclear magnetic resonance (NMR) data were recorded in $CDCl_3$ on a Varian Avance 400-MHz spectrometer. High performance liquid chromatography (HPLC) was performed with a Waters 590 system (Milford, MA) coupled to a Shimadzu SPD UV-Visible detector (Columbia, MD) and a gamma counting in-line radiation flow

Revision

detector (Model 105s, CRA; Berkeley, CA). The HPLC data was collected with a SRI Peaksimple, model 304, data system (Torrance, CA). Counting of tissue and blood samples utilized a Hidex automated gamma counter (Turku, Finland).

Male Sprague-Dawley rats (250-400 g; Charles River, Inc., Skokie, IL) were used for the [^{11}C]2-PAM biodistribution, blood and PET imaging studies. The animals were cared for and used at the University of California, San Francisco (UCSF) facilities that are accredited by the American Association for Accreditation of Laboratory Animal Care (AAALAC). The animal studies adhered to UCSF IACUC approved protocols that satisfied NIH guidelines and institutional regulations. Prior to injection of [^{11}C]2-PAM, rats were lightly anesthetized (~1-2% isoflurane) and lateral tail vein catheters were installed in the lower tail portion. The catheter line was flushed with 200 µL of saline and capped. Thereafter, the catheter cap was removed and tracer was injected as a bolus and then the catheter was flushed with 0.3 mL saline.

Synthesis of 2- pyridinealdoxime methiodide (2-PAM) under limiting methyl iodide reagent conditions. 2-Pyridinealdoxime (10 mg; 0.082 mmol) was dissolved in 200 µL DMF at 125 °C or CH_3CN at 80 °C and added drop wise to a solution of methyl iodide (2.0 µL) in 50 µL DMF or CH_3CN over 5 min. After the addition, the reaction was kept at the indicated temperature for 5 min. The percent conversion to 2-PAM was 80-90% (DMF) and 35-40% (CH_3CN) as determined by NMR integration of aldoxime CH=N peaks or by the ratio of the N-CH_3 to aromatic region in d_6-DMSO. Conversion to 2-PAM in CH_3CN was 40 ±

Revision

4% (using 2-PAM as internal standard) as measured by reversed-phase HPLC (UV at 290 nm) following evaporation of the solvent *in vacuo* using a Sonoma C_{18}(2) 5μ 100Å 15cm x 4.6mm (ES Industries; West Berlin, NJ) with a mobile phase of 10% C_2H_5OH/10 mM 2-(N-morpholino)ethanesulfonic acid in H_2O at 1.0 mL/min.

Radiosynthesis of [^{11}C]2-PAM. 2-Pyridinealdoxime (1-10 mg) is dissolved in 300 μL of anhydrous CH_3CN in a 4 mL 1-dram vial and sealed with a Teflon-lined silicone septum screw-cap. Utilizing a gas-phase method[16] and a GE Tracerlab FX C Pro radiosynthesis box, [^{11}C]CH_3I was produced then bubbled into the CH_3CN solution and the reactor vial was sealed. The mixture was heated at 80-140 °C for 8 min on an aluminum block heater. The reactor vial was removed from the heating source and allowed to cool for 60 seconds. The cap was removed, the CH_3CN solution was diluted with 2.5 mL of saline, and the crude material was injected onto a 10 x 250 mm, 10 μm Hamilton PRP-1 HPLC column. The HPLC purification used saline as mobile phase at a flow rate of 3 mL/min, with a retention time of [^{11}C]2-PAM at 8.5 min (see Supporting Information, Chromatograms section for representative HPLC elution profiles, and the Additional Radiolabeling Studies for [^{11}C]2-PAM Production section).

Dose Formulation. Doses of [^{11}C]2PAM were formulated in sterile isotonic saline (pH ~ 7) as 100-200 μCi in 1.0-1.5 mL for the biodistribution and blood determinations, and also 0.5-1.0 mCi in 0.5-1.0 mL for the PET imaging evaluations; in which the average dose volume across both sets of experiments

Revision

was ~ 1.0 mL. Before animal dosing, quality control of the dosing was accomplished by analytical HPLC (7µm Hamilton PRP-1 4.6 x 250 mm flow rate 1mL/min) demonstrating >99% radiochemical purity and >95% chemical purity. In separate experiments, doses were allowed to remain at room temperature for 2 h, and then subjected to reversed-phase analytical HPLC analysis (see Supporting Information).

Rat Biodistribution Studies. Rats received a bolus injection of 100-200 µCi of [^{11}C]2-PAM via tail vein catheter port followed by a 0.3 mL saline flush. Rats were euthanized by lateral chest puncture under anesthesia and dissected at 2, 5, 10, 30, and 60 min after injection (n = 3 per time point). Blood was collected by cardiac puncture immediately prior to euthanasia at each time point. Whole organs of brain, liver, heart, kidneys, lungs, bone (femur) and blood were collected into 20 mL pre-weighed glass scintillation vials and capped, where they were placed into a Hidex automated gamma counter (Hidex AMG) to be counted and weighed. Decay corrected data was exported from the Hidex instrument to Excel (Microsoft Office) software and plotted as decay corrected percent injected dose per gram (% ID/g) ± SEM versus time (min). To compare the % ID/g values of the two tracer dose regimens (i.e., tracer alone and tracer in the presence of 30 mg/kg of cold 2-PAM) one-way ANOVA analyses were performed for each tissue and blood using R software (version 3.0 or later).

Revision

Calculated Estimates of Blood Activity in Biodistribution Rat Brain Tissues. Rat blood and brain tissue biodistribution radioactivity data from 2-60 min were analyzed to estimate the amount of the percent contribution of blood signal in brain tissue. Everett[19] previously reported that average-sized rat brain blood volume is ~30-35 μL/g of tissue. Using a mid-range brain blood volume of 32.5 μL/g (equal to 0.0325 mL/g), and blood and brain % ID/g values per time point (Figure 2; per Supporting Information, Numerical Blood and Brain Data) with a blood density of 1 g/mL afforded the following relationships (Eqn 1-2) and ratio (Eqn 3), where t = time point measured (for example at t_1):

blood at t_1 (% ID/g) = blood % ID/g at at t_1 x 1 g/1mL x 0.0325 mL/g (Eqn 1)

brain at t_1 (% ID/g) = brain % ID/g at t_1 (Eqn 2)

% of blood in brain tissue at t_1 (% ID/g) =

blood at t_1 (% ID/g) / brain at t_1 (% ID/g) x 100 (Eqn 3)

Rat Arterial Blood Metabolites. Rats were installed with a tail artery catheter at the upper tail region for blood sampling and the catheter was flushed with saline heparin solution prior to blood collection. Tracer (1-3 mCi) was injected via a lower tail vein catheter and then 5 min later arterial blood (100 μL) was collected by heparin treated syringe. Blood samples were placed in heparin treated plastic 1.5 mL snap-lid vials containing 10 μL of 10 mg/mL citric acid, centrifuged at 13,200 g

Revision

for 1 min and remaining supernatant was removed and placed in a second tube. The supernatant was treated with 100 μL of acetonitrile to precipitate protein, the protein pellet was removed after centrifugation and the serum supernatant was collected. Chromatographic separation of serum radioactive components was conducted by preparative thin layer chromatography (TLC, 3.5 x 10 cm aluminum-backed silica with fluorescent indicator (254 nm), mobile phase = *n*-butanol:acetic acid:water (5:1:3)) to accommodate the carbon-11 half-life. The chromatography was run in parallel with known cold chemical metabolite standards[12, 15, 20] that were prepared in house by literature methods.[25, 26] Co-migration of standards with radioactive spots were excised with scissors, placed in 20 mL glass scintillation vials and counted with the Hidex gamma counter. The data was exported from the Hidex instrument to Excel (Microsoft Office) software and reported as relative % of total radioactivity, defined as the decay corrected ratio of component radioactivity over the sum of all radioactivity counted across the samples x 100.

Rat PET-CT and MR Imaging Studies. Tracer [^{11}C]2-PAM i.v. bolus doses of 0.5-2.0 mCi as formulated in 0.5-2.0 mL of saline were administered. The cold 2-PAM PET imaging experiments were accomplished by co-injecting 2-PAM at 30 mg/kg, saline (1-2 mL) with tracer. The PET, CT, and MR imaging were performed northermic (37 ˚C) under isoflurane anesthesia (1-1.5 %). The PET and CT imaging data were acquired with a Siemens Inveon microPET/CT scanner system (*ca.* 1.5 mm PET imaging spatial resolution). Dynamic PET imaging data were acquired over 30 min beginning ~0.5 min after the time of injection of tracer. The

Revision

PET data were reconstructed with using a Siemens Inveon reconstruction program suite, including OSEM2D; as 6 frames, 300 seconds per frame for the 30 min scans, decay time corrected, and quantified with a radiation phantom instrument calibration factor. A partial volume correction was not applied, and conservative ROI definitions were used as described below. The CT data were acquired in standard rat mode: 80 kVp, 225 mA; 400 ms exposure, 194 steps x 194 degrees, and 97-micron isotropic resolution. The MR data were acquired with a Bruker Biospin 7-Tesla magnet, using a multi-slice 2D FLASH protocol with the following parameters: T2*-weighted gradient recall echo, TR = 1528.3 msec, TE = 7 msec, and 256 x 256 x 50 voxels, affording 16 μm^3 resolution.

The reconstructed MR, CT and PET imaging data files were processed with AMIDE open source software[27] (SourceForge), version 1.0.4 (or later versions). The MR and CT images were oriented as defined by Paxinos[21, 22] and Walker[23]. Cranial landmarks of bregma and lambda were identified from the CT images. The X, Y, Z coordinates of imaging views were centered at bregma, equivalent to the origin of the first scan, then consistent landmark structures were iteratively co-registered and template fit against the cranial structures of the first scan landmarks. Subsequently, the landmarks were correlated with cerebral soft tissues from the MR scans.

The co-registered imaging data permitted regions of interest (ROIs) (Figures 5-7) to be defined within their ROI volume size limits and locations, and against established stereotaxic three-dimensional locations.[21-23] The ROIs were defined as follows: whole brain, heart, lung, kidney and liver. PET scan regional

Revision

tissue radioactivity is reported as Standardized Uptake Value (SUV) defined as: [activity concentration in the tissue region of interest (MBq/cc) / decay corrected injected dose at time = 0 (MBq)] x body weight of the rat as gram (g).[24] ROI PET scan statistics (SUV ± SEM) collected from time points at mid-frame were exported to Excel (Mircrosoft Corp.) and plots of SUV versus time were generated using either Excel or GraphPad Prism (La Jolla, CA) software.

ASSOCIATED CONTENT

Supporting Information

Chromatograms of the reversed-phase HPLC UV and radioactivity detection profiles of the semi-preparative crude material tracer purification and similar analytical HPLC profiles are shown. A limited series of pyrido-2-aldoxime precursor, solvent (DMF, CH_3CN), temperature and time radiolabeling trials reporting radiochemical yield and purity is given. Enhanced views of the Figure 5, baseline (tracer alone) and tracer co-injected with 30 mg/kg cold 2-PAM, time-activity curves in rat are provided. Numerical data from the baseline blood and brain tissue biodistribution experiments (Figure 2) are given. This material is available free of charge via the Internet at http://pubs.acs.org.

AUTHOR INFORMATION

Corresponding Author

Revision

*Mailing address: Department of Biomedical and Pharmaceutical Sciences, University of Montana, Missoula. MT, 59812-1552. Phone: 406-243-4984. E-mail: john.gerdes@umontana.edu

Author Contributions

C.M.T. and J.M.G designed the tracer. C.M.T. and N.G. performed the cold alkylation studies, and prepared the non-radioactive tracer and metabolite standards. K.D.N., J.E.B. and H.F.V. developed the radiosynthesis, K.D.N.,J.E.B. and T.R.H produced [^{11}C]2-PAM, and performed the rodent imaging, biodistribution studies and blood metabolite analyses with T.H . C-K.C. with J.M.G. performed the PET imaging analyses; J.M.G., and C.M.T, wrote the manuscript with contributions provided from C-K. C., K.D.N., T.R.H. and H.V.B. All authors reviewed the manuscript.

Funding

Research reported in this publication was supported by the National Institute Of Neurological Disorders And Stroke of the National Institutes of Health under Award Number U01NS092495. The content is solely the responsibility of the authors and does not necessarily represent the official views of the National Institutes of Health.

Notes

The authors declare no competing financial interest.

Revision

ACKNOWLEDGEMENTS

We are grateful for support from the NIH and the expert radiochemical technical assistance of Ms. Salma Jivan of the Department of Radiology and Biomedical Imaging at the University of California, San Francisco.

ABBREVIATIONS

ACh, acetylcholine; AChE, acetylcholinesterase; ANOVA, analysis of variance; bio-d, biodistribution; BBB, blood-brain barrier; CH_3CN, acetonitrile; CNS, central nervous sytem; CT, micro-computed axial tomography; DMF, dimethylformamide; DMSO, dimethyl sulfoxide; HPLC, reversed-phase high performance liquid chromatography; ID, injected dose; i.v., intravenous; MR, magnetic resonance; min, minutes; NMR, nuclear magnetic resonance; 2-PAM, 2-pyridinealdoxime methiodide; P2S, 2-pyridinealdoxime methyl methanesulfonate; PET, positron emission tomography; PK, pharmacokinetic; OP, organophosphate; OP-AChE adduct, phosphorylated acetylcholinesterase; RCY, radiochemical yield; ROI, region of interest; SD, standard deviation; SEM, standard error measures; SUV, standardized uptake value; TAC, time-activity curve; TLC, thin-layer chromatography; UV, utlraviolet.

REFERENCES

Revision

[1] Jokanovic, M. (2012) Structure-activity relationship and efficacy of pyridinium oximes in the treatment of poisoning with organophosphorus compounds: a review of recent data, *Curr Top Med Chem 12*, 1775-1789.

[2] Jokanovic, M., and Prostran, M. (2009) Pyridinium oximes as cholinesterase reactivators. Structure-activity relationship and efficacy in the treatment of poisoning with organophosphorus compounds, *Curr Med Chem 16*, 2177-2188.

[3] Jokanovic, M., and Stojiljkovic, M. P. (2006) Current understanding of the application of pyridinium oximes as cholinesterase reactivators in treatment of organophosphate poisoning, *Eur J Pharmacol 553*, 10-17.

[4] Shih, T. M., and McDonough, J. H., Jr. (1999) Organophosphorus nerve agents-induced seizures and efficacy of atropine sulfate as anticonvulsant treatment, *Pharmacol Biochem Behav 64*, 147-153.

[5] Gilat, E., Goldman, M., Lahat, E., Levy, A., Rabinovitz, I., Cohen, G., Brandeis, R., Amitai, G., Alkalai, D., and Eshel, G. (2003) Nasal midazolam as a novel anticonvulsive treatment against organophosphate-induced seizure activity in the guinea pig, *Arch Toxicol 77*, 167-172.

[6] Reddy, S. D., and Reddy, D. S. (2015) Midazolam as an anticonvulsant antidote for organophosphate intoxication--A pharmacotherapeutic appraisal, *Epilepsia 56*, 813-821.

[7] Eddleston, M., Buckley, N. A., Eyer, P., and Dawson, A. H. (2008) Management of acute organophosphorus pesticide poisoning, *Lancet 371*, 597-607.

Revision

[8] Bodor, N., Shek, E., and Higuchi, T. (1976) Improved delivery through biological membranes. 1. Synthesis and properties of 1-methyl-1,6-dihydropyridine-2-carbaldoxime, a pro-drug of N-methylpyridinium-2-carbaldoxime chloride, *J Med Chem 19*, 102-107.

[9] Bodor, N., Shek, E., and Higuchi, T. (1975) Delivery of a quaternary pyridinium salt across the blood-brain barrier by its dihydropyridine derivative, *Science 190*, 155-156.

[10] Hobbiger, F., and Vojvodic, V. (1967) The reactivation by pyridium aldoximes of phosphorylated acetylcholinesterase in the central nervous system, *Biochem Pharmacol 16*, 455-462.

[11] Sakurada, K., Matsubara, K., Shimizu, K., Shiono, H., Seto, Y., Tsuge, K., Yoshino, M., Sakai, I., Mukoyama, H., and Takatori, T. (2003) Pralidoxime Iodide (2-PAM) Penetrates across the Blood-Brain Barrier, *Neurochemical Research 28*, 1401-1407.

[12] Firemark, H., Barlow, C. F., and Roth, L. J. (1964) The Penetration of 2-Pam-C14 into Brain and the Effect of Cholinesterase Inhibitors on Its Transport, *J Pharmacol Exp Ther 145*, 252-265.

[13] Petrikovics, I., Papahadjopoulos, D., Hong, K., Cheng, T. C., Baskin, S. I., Jiang, J., Jaszberenyi, J. C., Logue, B. A., Szilasi, M., McGuinn, W. D., and Way, J. L. (2004) Comparing therapeutic and prophylactic protection against the lethal effect of paraoxon, *Toxicol Sci 77*, 258-262.

[14] Shih, T. M., Skovira, J. W., O'Donnell, J. C., and McDonough, J. H. (2010) In vivo reactivation by oximes of inhibited blood, brain and peripheral tissue

cholinesterase activity following exposure to nerve agents in guinea pigs, *Chem Biol Interact 187*, 207-214.

[15] Poziomek, E. J., Hackley, B. E., and Steinberg, G. M. (1958) Pyridinium Aldoximes1, *The Journal of Organic Chemistry 23*, 714-717.

[16] Larsen, P., Ulin, J., Dahlstrøm, K., and Jensen, M. (1997) Synthesis of [11C]iodomethane by iodination of [11C]methane, *Applied Radiation and Isotopes 48*, 153-157.

[17] Jovanovic, D. (1989) Pharmacokinetics of pralidoxime chloride. A comparative study in healthy volunteers and in organophosphorus poisoning, *Arch Toxicol 63*, 416-418.

[18] Gupta, R. C. (2015) *Handbook of toxicology of chemical warfare agents*, Second edition. ed., Elsevier/AP, Academic Press is an imprint of Elsevier, Amsterdam ; Boston.

[19] Everett, N. B., Simmons, B., and Lasher, E. P. (1956) Distribution of blood (Fe 59) and plasma (I 131) volumes of rats determined by liquid nitrogen freezing, *Circ Res 4*, 419-424.

[20] Enander, I., Sundwall, A., and Sorbo, B. (1962) Metabolic studies on N-methylpyridinium-2-aldoxime. III. Experiments with the 14C-labelled compound, *Biochem Pharmacol 11*, 377-382.

[21] Paxinos, G. (2015) Preface, In *The Rat Nervous System (Fourth Edition)*, p xi, Academic Press, San Diego.

[22] Paxinos, G., and Watson, C. (2007) *The rat brain in stereotaxic coordinates*, 6th ed., Academic Press/Elsevier, Amsterdam ; Boston ;.

Revision

[23] Walker, W. F. H., Dominique G. (1997) *Anatomy and Dissection of the Rat*, 3rd edition ed., Freeman, W. H. & Company, New York.

[24] Gambhir, S. S. (2004) Quantitative Assay Development for PET, In *Molecular Imaging and its Biological Applications* (Phelps, M. E., Ed.), pp 130-132, Springer, New York, NY.

[25] Ellin, R. I. (1958) Stability of Pyridine-2-aldoxime Methiodide. I. Mechanism of Breakdown in Aqueous Alkaline Solution, *Journal of the American Chemical Society 80*, 6588-6590.

[26] Ellin, R. I., Carlese, J. S., and Kondritzer, A. A. (1962) Stability of pyridine-2-aldoxime methiodide II. Kinetics of deterioration in dilute aqueous solutions, *Journal of Pharmaceutical Sciences 51*, 141-146.

[27] Loening, A. M., and Gambhir, S. S. (2003) AMIDE: a free software tool for multimodality medical image analysis, *Molecular imaging 2*, 131-137.

Table of Contents Graphic